Deciphering the dynamical chromosome structural reorganizations in human neural development

Xiakun Chu [1,2,3,*] Cibo Feng [1] and Jin Wang [4,5,†]

[1]*Advanced Materials Thrust, Function Hub, The Hong Kong University of Science and Technology (Guangzhou), Guangzhou, Guangdong 511400, China*

[2]*Guangzhou Municipal Key Laboratory of Materials Informatics, The Hong Kong University of Science and Technology (Guangzhou), Guangzhou, Guangdong 511400, China*

[3]*Division of Life Science, The Hong Kong University of Science and Technology, Clear Water Bay, Hong Kong SAR 999077, China*

[4]*Center for Theoretical Interdisciplinary Sciences, Wenzhou Institute, University of Chinese Academy of Sciences, Wenzhou, Zhejiang 325001, China*

[5]*Department of Chemistry and Physics, The State University of New York at Stony Brook, Stony Brook, New York 11794, USA*

(Received 19 December 2023; accepted 25 May 2024; published 21 June 2024)

Understanding the mechanisms of cell-fate determination in neural development is pivotal for advancing regenerative medicine and addressing neurodegenerative diseases. Cell-fate determination is controlled by the underlying gene expression networks, which are further regulated by the three-dimensional chromosome structures. During neural development, chromosomes progressively adapt their structures to accommodate the requisite gene expressions. However, elucidating the pathways of chromosome structural dynamics during these transitions remains a grand challenge. In this study, we employed the data-driven coarse-grained molecular dynamics simulations, coupled with the nonequilibrium landscape-switching model, to quantify the chromosome structural dynamics during human neural development. We focused on a simplified human neural developmental system, comprising of cell differentiation, reprogramming, and transdifferentiation among the neural progenitor cell (NPC), the glia cell, and the neuron cell. We identified significant large-scale chromosome structural reorganizations during cell-state transitions. From the chromosome structural perspective, the transdifferentiation processes between the glia and neuron cells exhibited nonmonotonic behaviors characterized by an initial increase followed by a subsequent decrease in cell stemness. The transdifferentiation appeared to share the same routes of differentiation after passing through the NPC. Additionally, our findings revealed that the chromosome structural dynamical pathways at the scale of topologically associating domains exhibited little overlap, in contrast to the ones at the long-range regions. This suggests that the active, ATP-driven molecular processes play dominant roles in modulating topologically associating domain (TAD) structures, while the compartmental segregation in chromosomes is primarily governed by the passive phase separation. Our study offers a theoretical exploration of neural cell-fate determination from the chromosome structural perspective, paving a way for potential applications in neuroregeneration.

DOI: 10.1103/PhysRevResearch.6.023309

I. INTRODUCTION

The emergence of cell functionality and the specification of cell types are fundamental aspects of cell development, encompassing processes such as cell differentiation, reprogramming and transdifferentiation. In the nervous system, these cell-fate determination processes play a pivotal role in the development and shaping of the brain, offering a potential therapeutic avenue for replenishing neuronal losses associated with neurodegenerative diseases and brain injuries [1]. Numerous attempts have made to convert non-neuronal cells into neurons, employing methods such as indirect reprogramming (followed by differentiation) or direct reprogramming (i.e., transdifferentiation) [2]. For instance, both mouse and human fibroblast (Fibro) cells have demonstrated to have the capability to directly convert into neurons using lineage-specific transcription factors or small molecules [3–5]. Significant progress has also been achieved in converting glia (Glia) cells into functional new neurons *in vivo*, both with and without passing through the proliferative progenitor stage [6–9]. However, due to the lack of the molecular-level understanding of cell development, several key questions remain unanswered, such as how to effectively control the cell-fate conversion process and enhance reprogramming efficiency in practical applications [10].

It is widely acknowledged that cell development is intricately regulated by the underlying gene regulation network. Serving as the structural scaffold for genes, the genome is highly compacted within the cell nucleus, maintaining a

*Contact author: xiakunchu@hkust-gz.edu.cn
†Contact author: jin.wang.1@stonybrook.edu

well-ordered three-dimensional (3D) organization to achieve specific gene expression patterns [11]. Determining the structure of genome has been a long-standing pursuit in molecular and cell biology, till the invention of chromosome conformation capture (3C) techniques [12]. Hi-C, as an advanced 3C method, typically measures the frequencies of contact formation between DNA segments throughout the genome in bulk samples containing millions of cells, resulting in an ensemble-averaged two-dimensional (2D) contact map [13]. Further analysis of the Hi-C contact map provides a hierarchical depiction of chromosome structure. At the megabase level, chromosomes organize into topologically associating domains (TADs). TADs represent domains of chromosomal loci that exhibit a higher rate of interactions within themselves compared to their interactions with surrounding domains. This structural characteristics makes TADs preferential structures for facilitating enhancer-promoter interactions [14–16]. At a larger scale (greater than 5 Mb), chromosomes segregate into two mutually exclusive regions known as compartment A and B. From the functional aspect, these regions strongly correlate with active euchromatin and inactive heterochromatin, respectively [13,17].

During the cell-state transition processes, chromosomes undergo extensive structural reorganizations, involving rearrangements of local TAD structures and compartment switching in long-range regions [18,19]. A comprehensive analysis of Hi-C data from the human embryonic stem cell (ESC) and their multilineage derivatives at early embryonic developmental stages revealed substantial A/B compartment switching, accompanied by corresponding changes in gene expressions [20]. In ESC differentiation, while TAD boundaries appear to be stable, interactions within TADs change significantly, exerting profound impacts on gene regulation [21]. Through the development of a high-resolution Hi-C technique [22], Bonev *et al.* measured the chromosome contact maps of the mouse ESC, the neural progenitor cell (NPC), and the cortical neuron cells. They observed global genome reorganizations at all scales during the mouse neural differentiation from the ESC, establishing a close relationship between chromosome structural adaptations and gene expression specifications in neural development. A recent Hi-C experiment focused on the human NPC, the Glia cell, and the neuron (Neuron) cell revealed that differentiation of the NPC into the Glia and Neuron cells was associated with widespread remodeling of chromosome interactions [23]. This underscores the significance of chromosome structural reorganizations in regulating neural development [24].

Despite the accumulation of Hi-C contact maps for chromosomes in individual cell types within the nervous system [20,25–27], comprehensive characterizations of dynamical chromosome structural reorganizations during cell-state transitions in cell development remains elusive. This impedes our understanding of the structure-function relationships at the chromosomal level during these dynamical processes. In this study, we focused on a simplified human neural developmental system comprising the NPC, the Glia cell and the Neuron cell. Using our previously developed landscapes-switching model [28–34], we established continuous connections between any pair of these three cell types and studied chromosome structural dynamics during the transitions through molecular dynamics (MD) simulations. Our analysis unveiled significant large-scale chromosome structural reorganizations occurring in human neural development. During transdifferentiation between the Glia and Neuron cells, we observed that chromosomes exhibit high structural similarity with those at the NPC, leading to an increase-followed-by-decrease behavior in cell stemness. Notably, we found that the forward and reverse pathways at the TAD scale exhibited little overlap, in contrast to those at the long-range scale. This implies that active, nonequilibrium molecular-level processes predominantly influence the modulation of the TAD structures. Our results offer valuable insights into the dynamical pathways of cell-state transitions in human neural development from the chromosome structural perspective. These findings contribute to our understanding of neural cell regeneration, providing potential implications for the treatment of neurodegenerative diseases.

II. MATERIALS AND METHODS

A. Hi-C data processing

The Hi-C data for the NPC, the Glia cell and the Neuron cell were obtained from an open-source platform (synapse, ID: syn12979101) [23]. The Hi-C data for the ESC and the Fibro cell were downloaded from the Gene Expression Omnibus (GEO) database with accession numbers GSE35156 [14] and GSE63525 [17], respectively. Read pairs were individually mapped to the reference human genome (hg19) and we used the standard pipeline of HIC-PRO (version 2.3.1) to process the raw Hi-C data [35]. The resulting contact matrices were further normalized using the iterative correction and eigenvector decomposition (ICE) method [36]. Here, we focused on the long arm of chromosome 14, covering a range of 20.5–106.1 Mb. The resolution of the Hi-C data was set to be 100 kb, resulting in 857 beads in the subsequent MD simulations. As noted in previous studies [37,38], each bead at this resolution approximately represents a 30-nm chromatin fiber. In the 30-nm chromatin fiber, nucleosomes are assumed to be helically packed, forming arrays that exhibit chain stiffness. We converted the contact frequency into the contact probability f_{ij} through further normalization, based on the fact that the neighboring beads have the highest contact frequencies and are always in contact with probability $f_{ii\pm1} \equiv 1$ in the beads-on-a-string model.

B. Polymer model

In the absence of Hi-C data for training, chromosomes in the coarse-grained MD simulations were initially described by a generic homopolymer model, which comprises of bonded and non-bonded potentials [39]. The potential of the homopolymer model is expressed as

$$V_{\text{Homopolymer}} = V_{\text{Bonds}} + V_{\text{Angles}} + V_{\text{sc}} + V_{\text{C}}.$$

The bond potential, denoted as V_{Bonds}, is composed of two elements: the finitely extensible nonlinear elastic (FENE) potential, represented as V_{FENE} [40], and a hard-core potential, labeled as V_{hc}, which serves to prevent spatial overlap.

Mathematically, V_{Bonds} is expressed as

$$V_{\text{Bonds}} = V_{\text{FENE}} + V_{\text{hc}}.$$

The angle potential, denoted as V_{Angles}, acts on three consecutive beads $(i-1,\ i,\ i+1)$ and is responsible for maintaining the stiffness of the chain [39]. For nonbonded interactions between beads i and j ($|i-j|>1$), the soft-core potential V_{sc} is employed, modeling the effects of topoisomerase enzymes that play an important role in untangling DNA chains [38,41,42]. The spherical confinement potential, denoted as V_{C}, models the effects of the nuclear membrane, ensuring that the chromosome occupies the appropriate volume fraction within the cell nucleus, set at 10%. V_{C} functions such that if the distance of any bead in the polymer from the center of the sphere exceeds the defined radius, it will be pulled back toward the center.

C. Maximum entropy principle simulations

We used a maximum entropy principle (MEP) strategy to incorporate the Hi-C data for a specific cell state into the aforementioned homopolymer model. According to MEP, the biasing potential ($V_{\text{Hi-C}}$) introduced should be in a linear form of the experimental observations [43]. Consequently, $V_{\text{Hi-C}}$ is expressed as

$$V_{\text{Hi-C}} = \sum_{i,j} \alpha_{ij} P_{ij},$$

where P_{ij} denotes the contact probability between the chromosomal loci "i" and "j", and α_{ij} acts as a prefactor modulating the strength of the biasing potential. In practice, P_{ij} was calculated using a step function [38,42]. The calculation of P_{ij} involved collecting all chromosome structures at a specific cell state or time point during the simulations.

The values of α_{ij} are determined iteratively through multiple rounds of MD simulation, aiming to minimize the discrepancy between the contact probabilities obtained from the simulated chromosome ensembles and the experimental data. Therefore, the final potential governing the chromosome structure and dynamics at the specific cell state is expressed as

$$V(\text{Cell}) = V_{\text{Homopolymer}} + V_{\text{Hi-C}}.$$

For detailed expressions and parameters of the model, please refer to our previous studies [28–34] and elsewhere [38,42,44].

D. Landscape-switching model

In order to investigate the chromosome structural dynamics during cell-state transitions in neural development, we used the landscape-switching model developed in our previous studies [28–34]. In brief, the model involves three main steps. (1) Initial cell-state simulation: we simulated the chromosome under the potential specific to the initial cell state, denoted as $V(\text{Cell}_{\text{Ini}})$. This potential was obtained from MEP simulations trained by the corresponding experimental Hi-C data. (2) Landscape-switching: We then switched the potential from the initial cell state to the destined cell state, represented as $V(\text{Cell}_{\text{Ini}}) \rightarrow V(\text{Cell}_{\text{Des}})$, where $V(\text{Cell}_{\text{Des}})$ is the potential associated with the destined cell state. (3) Destined cell-state simulation: we simulated the chromosome under $V(\text{Cell}_{\text{Des}})$. The simulation allowed the system to relax on the post-switching energy landscape. The relaxation processes during this transition were collected and represented as the structural dynamical trajectories of the chromosome during the cell-state transition.

The rationale of our model is summarized briefly as follows. The cell-state transition is driven by a large amount of energy input, primarily from ATP hydrolysis [45]. This leads to the breaking of detailed balance in the system, resulting in nonequilibrium dynamics of the process. In reality, a cell resides at a stable state and the cell differentiation, reprogramming and transdifferentiation do not occur spontaneously. This implies that the inter-landscape hopping dynamics (cell-state transition) occur much more slowly than the intra-landscape dynamics (dwelling on a stable state), leading to nonadiabatic dynamics of the cell-state transition processes. Our landscape-switching model, which implements an instantaneous switch of two landscapes at initial and final cell states, naturally result in a non-adiabatic nonequilibrium process, consistent with the nature of the cell-state transition.

E. MD simulation protocols

We used GROMACS (version 4.5.7) software [46] with PLUMED (version 2.5.0) [47], to conduct the MD simulations. The simulations were performed using Langevin dynamics with a friction coefficient of $10\tau^{-1}$, where τ represents the reduced time unit. We used a time step of 0.0005τ in the simulations to integrate the dynamics of the system. In our simulations, the temperature was represented in the reduced energy unit (ϵ) by multiplying the Boltzmann constant. All simulations were conducted at a temperature of ϵ, unless explicitly specified. It is important to note that the temperature in these simulations does not directly correspond to real-world values but rather represents an environmental scale influencing the structural dynamics of the chromosome under the specified potential [38].

During each iteration of the MEP simulations to calibrate α_{ij}, we conducted 100 independent MD simulations starting from different initial chromosome structures. To enhance the sampling of the conformational space, we employed a simulated annealing technique in these individual simulations. Initially, the temperature was gradually reduced from 4ϵ to ϵ over the first 250τ of the simulation. Subsequently, the temperature was held constant at ϵ for the remaining time. The second half of the trajectory, spanning from 500τ to 1000τ, was collected for calculating the contact probability P_{ij}.

The MEP simulation generated an ensemble of chromosome structures for the NPC, the Neuron cell, and the Glia cell, respectively. To reduce the number of chromosome structures in the ensemble, we performed hierarchical clustering based on the pairwise distance similarity between chromosomal loci. For each cluster with a population greater than 0.3%, we selected the two chromosome structures with the closest distances to the center. This resulted in 244, 314, and 358 structures representing the chromosome structural ensembles for the NPC, the Neuron cell, and the Glia cell, respectively.

Using the structures obtained from the aforementioned approaches, we conducted hundreds of independent simulations using the landscape-switching model for each cell-state transition process during neural development. Initially, the equilibration simulations under the potential of the initial cell state $V(\text{Cell}_{\text{Ini}})$ ran for a duration of 5000τ. Subsequently, a sudden switch of the potential from the initial cell state $V(\text{Cell}_{\text{Ini}})$ to the destined cell state $V(\text{Cell}_{\text{Des}})$ was implemented. Finally, simulations under the potential $V(\text{Cell}_{\text{Des}})$ were conducted for a duration of 1000τ.

Consequently, we generated 244 trajectories each for the NPC differentiation processes to the Neuron cell and the Glia cell, as well as 314 and 358 trajectories for the reprogramming processes of the Neuron cell and the Glia cell to the NPC. Additionally, we obtained 314 and 358 trajectories for the Neuron cell transition to the Glia cell and from the Glia cell transition to the Neuron cell, respectively. All trajectories were collected to perform analyses presented in the study. The data regarding the ESC and the Fibro cell (e.g., MEP simulations, landscape-switching simulations, etc.) were directly taken from our previous study [31].

F. Trajectory analysis

Due to the stochastic nature of individual cells [48], chromosome structures at the single-cell level are highly heterogeneous. We calculated ensemble-average contact maps P_{ij}, which were further used to describe the cell states from the chromosome structural perspective. The correlation between two contact probability maps was determined using the coefficient of determination R^2, defined as follows:

$$R^2 = 1 - \sum_{i,j}[P_{ij}(t) - P_{ij}(\text{Cell})]^2 \Bigg/ \sqrt{\sum_{i,j}[P_{ij}(t) - \langle P_{ij}(t)\rangle]^2 \sum_{i,j}[P_{ij}(\text{Cell}) - \langle P_{ij}(t)\rangle]^2}.$$

Here, R^2 quantifies the similarity of the two contact maps P_{ij} at time t and the cell state Cell, where Cell stands for the NPC, Neuron cell, Glia cell, Fibro cell and ESC, respectively. A value of 1.0 for R^2 indicates identical contact maps, where $P_{ij}(t) = P_{ij}(\text{Cell})$. R^2, calculated without any offsetting, accumulates the deviation of every element between $P_{ij}(t)$ and $P_{ij}(\text{Cell})$, providing a quantitative measure of similarity or dissimilarity between these two matrices. When comparing the contact maps of the states I and J during the cell-state transition processes, $R^2(I, J)$ was calculated, where I and J represent times t^A and t^B, respectively. Any deviation of R^2 from 1.0 reflects the degree of difference between these two contact maps. To enable a more meaningful comparison, we calculated R^2 based on the distance-corrected contact maps. Specifically, we derived the distance-corrected contact maps from the normal contact maps by subtracting their average contact probability at the corresponding genomic distance [49].

To assess the formation of TADs, we applied the insulation score method as introduced by Crane *et al.* [50]. Following the methodology outlined in the original study, we utilized a sliding window size of 500 × 500 kb to calculate the insulation score based on the contact map. The minima on the insulation score profile were then used to identify the boundaries of TADs [50]. To quantify the degree of interaction enhancement, we calculated the enhanced contact probability [13,20]. This probability was determined by dividing the observed contact probability, denoted as P_{obs}, by the expected contact probability, denoted as P_{exp}. The observed contact probability P_{obs} was obtained by summing the contact probabilities at a resolution of 100 kb within a 1 Mb region. On the other hand, the expected contact probability P_{exp} was calculated as the average contact probability between chromosomal loci separated by a specified genomic distance.

To assess the reversibility of pathways, we calculated the contact probability $P_{ij}(t)$ during the cell-state transition via a simple linear interpolation between the data of the initial (type A) and final (type B) cell states, as follows:

$$P_{ij}(t) = P_{ij}(A) + \frac{t - t^{\text{Begin}}}{t^{\text{End}} - t^{\text{Begin}}} \times [P_{ij}(B) - P_{ij}(A)].$$

Thus, the corresponding reverse pathways from the initial (type B) to final (type A) cell states can be calculated, as follows:

$$P_{ij}(t) = P_{ij}(B) + \frac{t - t^{\text{Begin}}}{t^{\text{End}} - t^{\text{Begin}}} \times [P_{ij}(A) - P_{ij}(B)].$$

This method allowed us to generate forward and reverse trajectories between every pair of the NPC, the Glia cell, and the Neuron cell, resulting in a total of six transitions. Similar analysis methods as described above were then performed on these trajectories.

III. RESULTS

A. Dynamical chromosome structural reorganizations during human neural development

We applied our previously developed landscapes-switching model [28–34], implemented within MD simulations, to investigate chromosome structural reorganizations during neural development. The landscape-switching model was performed in two steps. First, Hi-C data at individual cell states, including the NPC, the Glia, and Neuron cells, were trained using the maximum entropy principle (MEP) coarse-grained MD simulations to render the respective energy landscapes [38,42,51]. This energy landscape dictates chromosome structural organization and dynamics within each cell state (Figs. S1–S3 in Supplemental Material [52]). Second, to establish connections between two cell states in the neural developmental system, we triggered cell-state transitions through an energy-excitation-followed-by-relaxation implementation. This was realized by switching the energy landscape for chromosome structural dynamics from the initial to the final cell state during MD simulations. Conse-

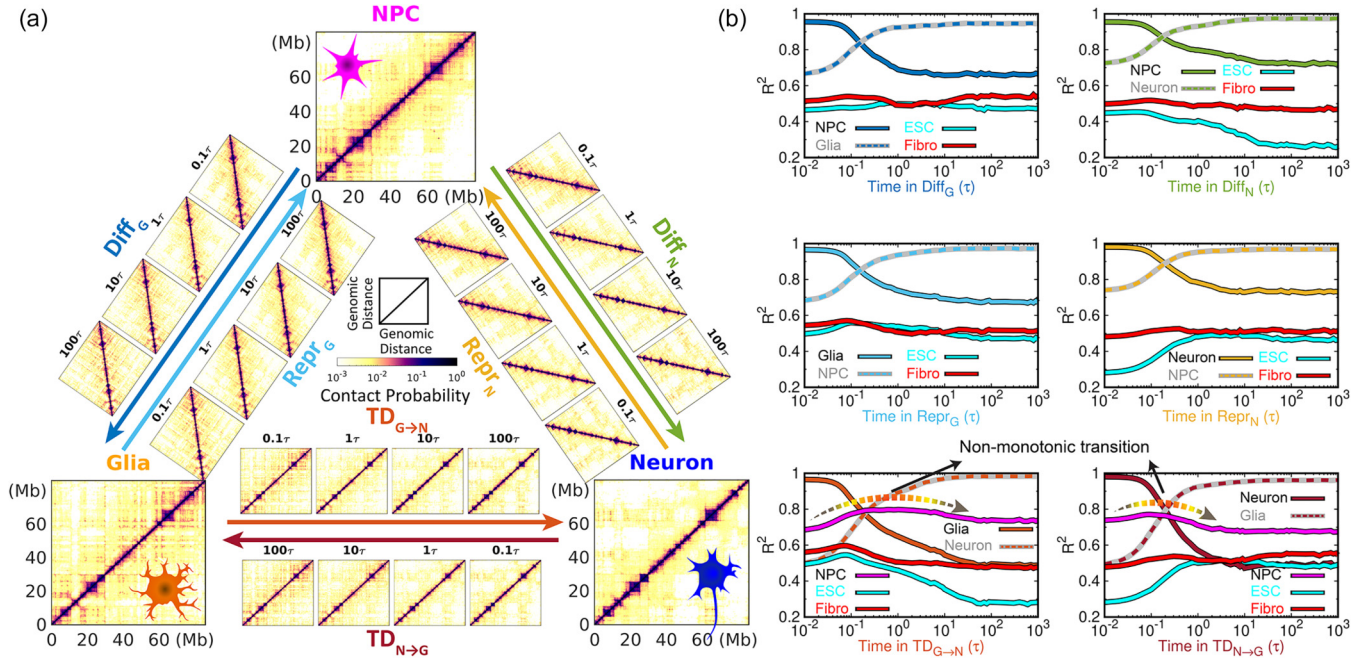

FIG. 1. Chromosome structural reorganizations during neural development. (a) Evolution of chromosome contact probabilities over time during cell-state transitions. The contact maps for the NPC and the Glia and Neuron cells are derived from experimental Hi-C data. Calculations for contact maps at $t = 0.1\tau$, 1τ, 10τ, and 100τ of each transition are performed, where τ represents the unit of MD time. The contact map resolution is 100 kb. (b) Correlation of the distance-corrected contact probability map during the transition with those at the initial (solid line) and final (dashed line) states of the transition, as well as the NPC (purple line), the ESC (cyan line), and the Fibro cell (red line) [49]. The degree of correlation is quantified by the coefficient of determination R^2, the full definition of which can be found in "Materials and Methods." Generally, a high (low) value of R^2 indicates a high (low) degree of similarity between two chromosome structures.

quently, there are six cell-state transition processes [Fig. 1(a)], including differentiation of the NPC to the Glia and Neuron cells ($\mathrm{Diff_G}$ and $\mathrm{Diff_N}$), reprogramming of the Glia and Neuron cells to the NPC ($\mathrm{Repr_G}$ and $\mathrm{Repr_N}$), and transdifferentiation between the Glia and Neuron cells ($\mathrm{TD_{G\to N}}$ and $\mathrm{TD_{N\to G}}$). Through the landscape-switching simulations, hundreds of parallel trajectories were generated for each cell-state transition process (details in "Materials and Methods"). Then, chromosome contact maps evolving with time were calculated by averaging all the trajectories at the same time points, mimicking the dynamic changes of Hi-C maps induced by cell-state transitions [Fig. 1(a)]. Due to the intimate structure-function relationships in chromosomes [20,53–56], the contact maps, which reflect the ensemble-average structural properties of chromosomes, can characterize the cell state during the transition processes from the chromosome structural perspective.

To see how chromosomes dynamically reorganize their structures, we calculated the similarities of the contact maps during cell-state transitions with respect to those at the NPC, the Glia cell, the Neuron cell, the ESC and the Fibro cell [Fig. 1(b)]. As the cell-state transition proceeds, the chromosome gradually adapt its structure, deviating from the one at the initial state and approaching towards the one at the final state. These chromosome structural adaptations are monotonic for all six cell-state transitions in neural development.

Throughout all the cell-state transitions in neural development, we observed that the chromosome structural similarities with respect to the ESC and the Fibro cell remain relatively low [Fig. 1(b), $R^2 < 0.6$, where R^2 is the coefficient of determination between the contact maps in the trajectories and contact maps of the ESC and the Fibro cell]. This indicates that chromosome structures within the neural system are quite different from those at the ESC and the Fibro cell. Thus, cell-state transitions within neural development do not approach the pluripotent state or the other terminally differentiated cell from the chromosome structural perspective.

For transdifferentiation between the Glia and Neuron cells, we observed that both the trends of R^2 with respect to the NPC along with time exhibit an increase-followed-by-decrease behavior [Fig. 1(b)]. This suggests that chromosomal structures during transdifferentiation may resemble those observed in the NPC. Considering that the NPC is a type of stem cell possessing the ability to differentiate into various types of cells within the central nervous system [57], it can be inferred that transdifferentiation between the Glia and Neuron cells initially enhances the degree of cell stemness and subsequently reduces it, from the chromosome structural perspective.

B. Cell-state transitions in human neural development from chromosome structural perspective

Our study focuses on six distinct cell-state transitions in neural development. Intuitively, the reprogramming processes initiated from the Glia and Neuron cells towards the NPC should merge during the transitions. Similarly, the processes of forming the Glia and Neuron cells through differentiation of the NPC and transdifferentiation should also merge at certain stages. To gain insights into how the merging of these two

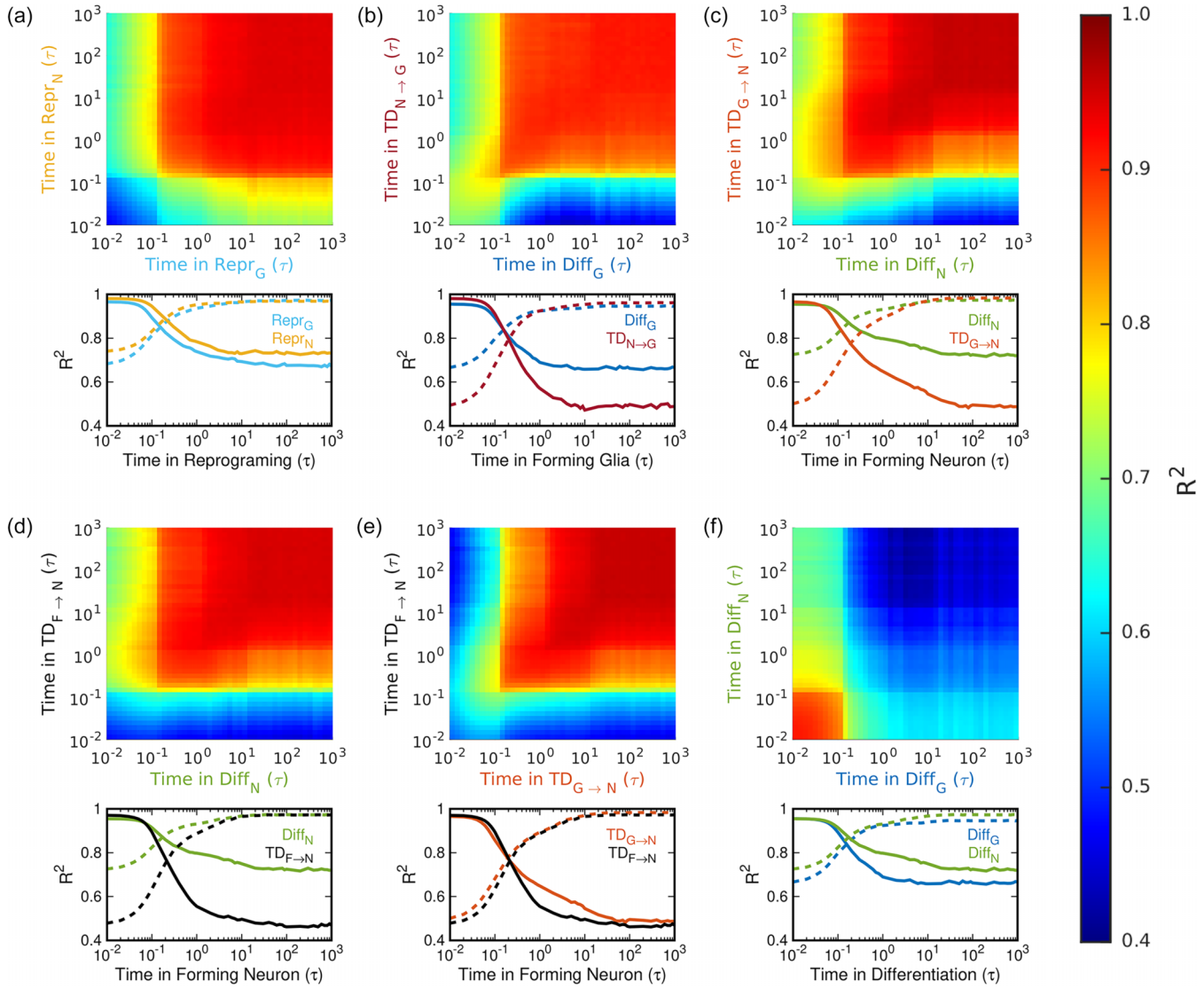

FIG. 2. Correlation maps illustrating time-evolving chromosome contact maps for two transitions during (a) reprogramming of the Glia and Neuron cells to the NPC (Repr_G and Repr_N), (b) transitions for forming the Glia cell from the NPC (differentiation, Diff_G) and the Neuron cell (transdifferentiation, $\text{TD}_{N\to G}$), (c) transitions for forming the Neuron cell from the NPC (differentiation, Diff_N) and the Glia cell (transdifferentiation, $\text{TD}_{G\to N}$), (d) transitions for forming the Neuron cell from the NPC (differentiation, Diff_N) and Fibro (transdifferentiation, $\text{TD}_{F\to N}$), (e) transitions for forming the Neuron from the Glia cell (transdifferentiation, $\text{TD}_{G\to N}$) and the Fibro cell (transdifferentiation, $\text{TD}_{F\to N}$) and (f) differentiation of the NPC to the Glia cell (Diff_G) and the Neuron cell (Diff_N). The comparison between the process "A" at time $t^A = I$ and the process "B" at time $t^B = J$ is performed by calculating the coefficient of determination $R^2(I, J)$ between the contact probabilities P_{ij} formed by the chromosomal loci i and j. $R^2(I, J)$ measures the similarity of two chromosome contact maps at time $t^A = I$ of the process A and $t^B = J$ of the process B ($R^2(I, J) = 1$ corresponds to identical contact maps with $P_{ij}(t^A = I) = P_{ij}(t^B = J)$, and the deviation of $R^2(I, J)$ from 1 indicates the degree of difference between these two contact maps). The *lower* panels in (a)–(f) show cell states "J" selected to be either the initial states (solid lines) or the final states (dashed lines), representing how chromosomes dynamically deviate from the initial structures and establish the final structures, simultaneously.

pathways occurs from the chromosome structural perspective, we calculated the coefficient of determination, R^2, between the two contact maps over time (Fig. 2).

For reprogramming, we observed that the pathways of the Glia and Neuron cells converting to the NPC become similar at approximately 0.5τ with high values of R^2 by comparing the chromosome structures during these two cell-state transitions [Fig. 2(a), *upper panel*, along the diagonal]. In other words, Repr_G and Repr_N share similar routes after 0.5τ, which can be approximately deemed as the merging point of these two pathways. At the merging point, the similarities of the contact maps to the destined NPC are high, close to 0.9 [Fig. 2(a), *lower panel*]. This implies that the reprogramming pathways of the Glia and Neuron cells only merge at the very late stage of the transitions when the contact maps at the merging point resemble those of the NPC. This observation of forming an NPC-like state from reprogramming of the Glia and Neuron cells is consistent with the previous experiments, where reprogramming of two terminally differentiated cells can lead to an ESC-like state prior

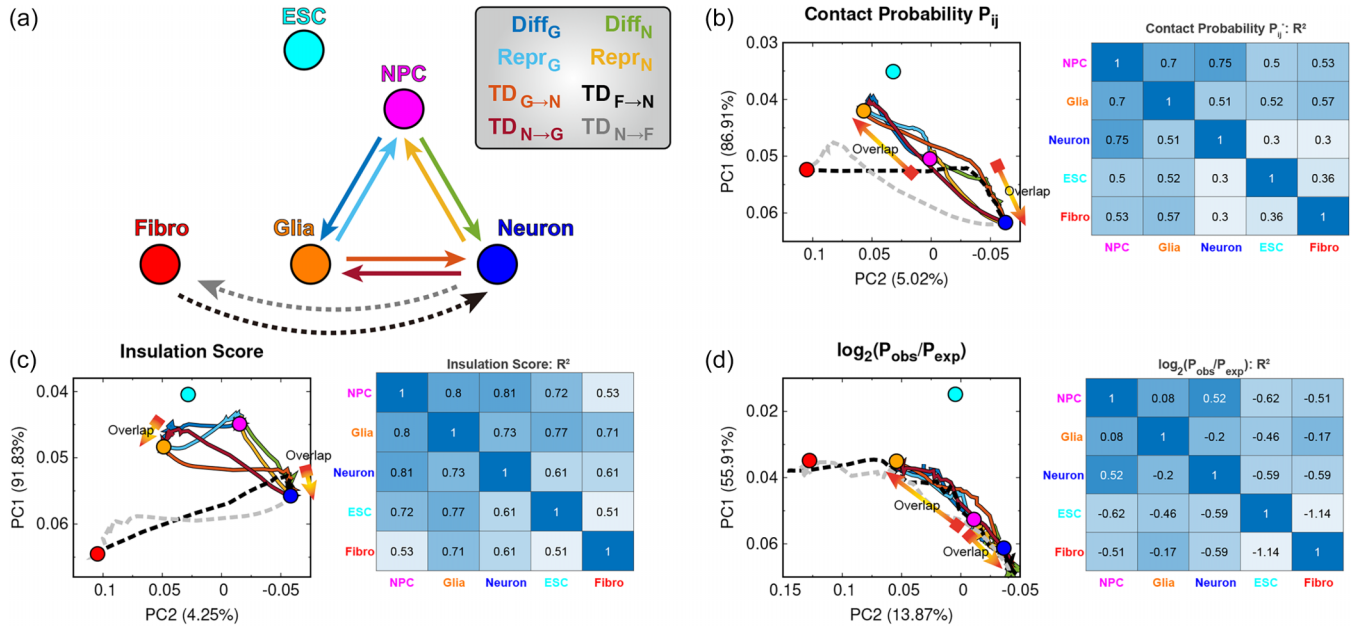

FIG. 3. Cell-state transitions in neural development from the chromosome structural perspective. (a) Illustration of the six cell-state transitions in neural development and two transitions between the Fibro and Neuron cells. (b) Quantified chromosome structural dynamical pathways depicted in PCA plots of contact maps projected onto the first two principal components (PCs, *left panel*). Percentages in axis labels represent the weight ratios of corresponding PCs and R^2 values showing the correlation between contact maps among the NPC, the Glia cell, the Neuron cell, the ESC, and the Fibro cell (*right panel*). (c) Similar to (b), but PCA plots and R^2 are based on the insulation score profiles [50]. (d) Similar to (b), but PCA plots and R^2 values are based on enhanced contact probability $\log_2(P_{\rm obs}/P_{\rm exp})$ [13,20].

to the establishment of the final induced pluripotent stem cell [58].

Interestingly, we observed distinct behaviors in adapting chromosome structures during differentiation and transdifferentiation towards the same destined cell, as compared to reprogramming processes. We found that the pathways of forming the Glia cell from the NPC differentiation and the Neuron cell transdifferentiation merge at approximately 0.1τ [Fig. 2(b), *upper panel*, along the diagonal], when the value of R^2 with respect to the destined Glia cell is smaller than 0.8 [Fig. 2(b), *lower panel*]. The results indicate that chromosomes are still structurally different from the ones within the Glia cell at the merging point, suggesting that the NPC differentiation and the Neuron cell transdifferentiation may share a similar route upon forming the Glia cell from the chromosome structural perspective. A similar phenomenon was observed for forming the Neuron cell from the NPC differentiation and the Glia cell transdifferentiation [Fig. 2(c)]. Notably, we observed that transdifferentiation from the Fibro to Neuron cells also shares the routes with the NPC differentiation and transdifferentiation from the Glia to Neuron cells [Figs. 2(d) and 2(e)]. Our results suggest that transdifferentiation can partially utilize the differentiation route to accomplish the cell-state transition from the chromosome structural perspective. This is reminiscent of a recent RNA-seq experimental observation that transdifferentiation from the Fibro to Neuron cells undergoes an NPC-like state [59]. Meanwhile, we compared the chromosome structural dynamics during the pathways of the NPC differentiation to the Glia and Neuron cells. We found that chromosomes during these two differentiation processes start to diverge from each other at approximately 0.1τ [Fig. 2(f), *upper panel*, along the diagonal], where chromosomes exhibit highly structural similarities to those at the NPC [Fig. 2(f), *lower panel*]. This observation aligns with emerging theoretical predictions and experiments, where cell differentiation processes initiated from stem cells to different sublineages bifurcates early [20,29,60].

C. Quantified chromosome structural dynamical pathways of human neural development

To understand the cell-state transitions during neural development at the chromosome structural level, we quantified the pathways through the PCA plots of different chromosome structural aspects (Fig. 3). Additionally, we included transdifferentiation pathways between the non-neural cell (i.e., the Fibro cell) and the Neuron cell, obtained from our previous work [31], into our following analysis [Fig. 3(a)]. Notably, the total weights of the first and second principal components (PC1 and PC2) in the PCA plots are relatively high, suggesting that projecting the high-dimensional simulation data onto only PC1 and PC2 is feasible and the relevant analyses should be reliable [Fig. 3(b)].

From the PCA plots of chromosome contact maps with a total weight of PC1 and PC2 at 91.93%, we observed nonoverlapping forward and reverse pathways for transitions between any pair of cell states [Fig. 3(b)]. By artificially generating interpolation-based transition trajectories connecting the initial and final cell states, we identified the direct correspondence between pathway overlap and reversibility (Fig. S4 in Supplemental Material [52]). Therefore, our observations based on the landscape-switching model underscore

the nonequilibrium nature of cell-state transitions, indicating their irreversibility of the processes. Notably, there is significant degree of overlap in the pathways of the NPC differentiation to the Glia cell ($\mathrm{Diff_G}$, blue line) and transdifferentiation of the Neuron cell to the Glia cell ($\mathrm{TD_{N\to G}}$, red line). This suggests that processes forming the Glia cell from different initial states may share a common route to gradually adapt chromosome structures. In contrast, the NPC differentiation pathways for forming the Neuron cell ($\mathrm{Diff_N}$, green line) exhibit only a small degree of overlap with the transdifferentiation pathways from the Glia to Neuron cells ($\mathrm{TD_{G\to N}}$, orange line) and the Fibro to Neuron cells ($\mathrm{TD_{F\to N}}$, dashed black line), highlighting the heterogeneity in pathways for forming different cell types. The PCA plots also indicate early bifurcation of the NPC differentiation pathways ($\mathrm{Diff_G}$, blue line; $\mathrm{Diff_N}$, green line) and late merging of reprogramming pathways ($\mathrm{Repr_G}$, cyan line; $\mathrm{Repr_N}$, yellow line), consistent with observations in Fig. 2.

To examine the dynamics of chromosome structural organizations at the TAD and compartment levels, we calculated the insulation score profiles and the enhanced contact probability $\log_2(P_{\mathrm{obs}}/P_{\mathrm{exp}})$ from the chromosome contact maps. Insulation score profiles were previously used to identify local TAD structures (details in "Materials and Methods") [50], while P_{obs} and P_{exp} are respectively the observed and expected contact probabilities with combined ratio of $\log_2(P_{\mathrm{obs}}/P_{\mathrm{exp}})$ describing the long-range compartment formation (details in "Materials and Methods") [13,20]. From the PCA plots of insulation score profiles and $\log_2(P_{\mathrm{obs}}/P_{\mathrm{exp}})$ with the respective total weights of PC1 and PC2 at 96.08% and 69.78% [Figs. 3(c) and 3(d)], we observed diverse behaviors in cell-state transition pathways during neural development from different chromosome structural aspects. The pathways of insulation score profiles revealed that merging points for pathways leading to the same cell types occur in the very late stages of cell-state transitions. This suggests that different cell-state transitions forming the same cell types may utilize different mechanisms to rearrange the TAD structures. Conversely, pathways from the PCA plots of $\log_2(P_{\mathrm{obs}}/P_{\mathrm{exp}})$ showed that merging of pathways leading to the same cell types can occur very early. For instance, the transdifferentiation pathway from the Neuron to Glia cells ($\mathrm{TD_{N\to G}}$, red line), projected onto $\log_2(P_{\mathrm{obs}}/P_{\mathrm{exp}})$, goes through the NPC. After passing through the NPC, the pathway of $\mathrm{TD_{N\to G}}$ in the PCA plots of $\log_2(P_{\mathrm{obs}}/P_{\mathrm{exp}})$ highly overlaps with that of the NPC differentiation to the Glia cell ($\mathrm{Diff_G}$, blue line). Intriguingly, we observed that the NPC is on the pathway of $\mathrm{TD_{F\to N}}$ (dashed black line) but deviates from $\mathrm{TD_{G\to N}}$ (orange line) in the PCA plots of $\log_2(P_{\mathrm{obs}}/P_{\mathrm{exp}})$. This implies that different neuron transdifferentiation processes may undergo different pathways, and the NPC is not the common intermediate state for those transitions.

The forward and reverse pathways for transitions between any pair of cell states appear to be nonoverlapped when projected onto the TAD structural formations. In contrast, the pathways projected onto the long-range structural interactions seem to be highly overlapped. Nonoverlapping TAD structural pathways reflect the irreversibility of cell-state transitions at local chromosome structural regions, emphasizing the nonequilibrium nature of TAD formation induced by ATP-dependent loop extrusion [61,62]. In contrast, the overlapping pathways in terms of $\log_2(P_{\mathrm{obs}}/P_{\mathrm{exp}})$ can be attributed to the fact that chromosome compartment segregation is largely formed by passive phase separation processes mediated by various proteins, such as transcription factors and heterochromatin protein 1 [63–65]. Our analyses of the quantified pathways contribute to the molecular-level understanding of how chromosomes dynamically reorganize their structures during cell-state transitions.

IV. DISCUSSION AND CONCLUSIONS

We employed a Hi-C data-driven approach, coupled with the landscapes-switching simulations, to investigate chromosome structural dynamics during cell-state transitions in human neural development. Our findings revealed large-scale chromosome structural reorganizations during these processes, emphasizing the intricate relationships between structure and function at the chromosomal level [19]. The developmental processes of cells can be illustrated through the Waddington's epigenetic landscape [60,66], where cell differentiation is metaphorically represented as a marble rolling from the upper level to the lower level of the landscape [Fig. 4(a)]. Triggered by external agents such as transcription factors or chemical stimulations, terminally differentiated cells can manipulate their fates back to the pluripotent state [67–71]. This phenomenon, known as cell reprogramming, is analogous to a marble climbing from the lower level to the upper level of Waddington's landscape [72]. Our simulations unveiled distinct pathways for differentiation and reprogramming regarding the reorganization of chromosome structures, emphasizing the nonequilibrium dynamic nature of cell developmental processes [73]. This suggests that cells utilize diverse molecular-level processes to achieve differentiation and reprogramming, respectively.

Notably, our simulations indicate nonoverlapping forward and reverse pathways predominantly at the TAD level. This implies that local chromosome structural dynamics, driven by various ATP-dependent molecular processes (e.g., loop extrusions [61,62], chromatin remodeling [74,75], etc.), contribute to the irreversibility of differentiation and reprogramming pathways. In contrast, highly overlapped chromosome structural reorganization pathways were observed at long-range regions for both differentiation and reprogramming, suggesting that passive molecular processes, such as phase separation, play a crucial role in establishing nonlocal chromosome structures [64,65]. Additionally, our observations indicate that the establishments of local chromosome structures precede those of nonlocal ones (Fig. S5 in Supplemental Material [52]). These findings are consistent with the relaxation dynamics of the Rouse-like polymer models [76,77]. Importantly, previous Hi-C experiments on cell-cycle processes also detected a faster recovery of TAD structures than that of compartment segregation during the mitosis-to-G1 transitions [78,79]. Collectively, our results suggest that chromosome structural reorganizations during cell developmental processes are initiated by active molecular processes at the local level, followed by passive molecular processes at the long-range level.

Cell transdifferentiation does not go through the ESC to achieve the cell-state transition between two terminally

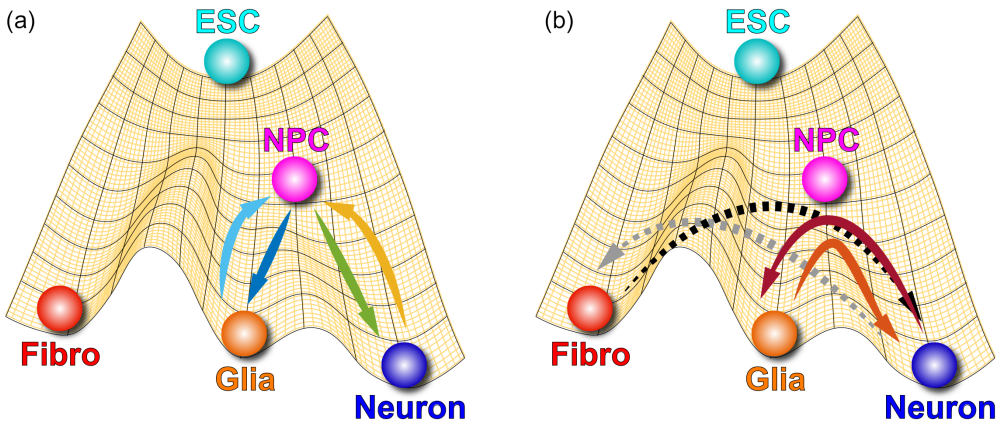

FIG. 4. A scheme illustrating cell-state transitions among the NPC, Glia, and Neuron cells for neural development on pictorial Waddington's landscapes from the chromosome structural perspective. *Left panel*: the differentiation and reprogramming processes. *Right panel:* the transdifferentiation processes, with transitions between the Fibro and Neuron cells shown with dashed lines.

differentiated cell types, thus it is less time-consuming and capable of reducing the risk of tumorigenesis [80–82]. We found that transdifferentiation can approach the NPC, though not the ESC, to accomplish cell-state transitions from the chromosome structural perspective. After passing through the NPC, transdifferentiation and differentiation may share the same route to accomplish the processes. Our theoretical results align with a previous experimental study [59], where transdifferentiation from the Fibro to Neuron cells can go through an NPC-like stage with several NPC genes expressed. Here, we found that chromosome structures during transdifferentiation from the Neuron to Glia cells can be very similar to those at the NPC, implying that the NPC is the intermediate state for this cell-state transition. Our theoretical results, combined with experiments [83], suggest that although cell transdifferentiation can bypass the ESC to directly convert somatic cell types, cells during this process still have to go through a precursor that possesses a certain degree of stemness. From Waddington's landscape, cell transdifferentiation can be described as a nonmonotonic process that occurs by initially climbing up the mountain, followed by rolling down to another basin as a function of cell-fate maturation [Fig. 4(b)].

Our theoretical studies provided quantified pathways for the dynamical structural organizations of chromosomes during human neuron cell differentiation, reprogramming, and transdifferentiation, thus contributing significantly to understanding neural developmental processes from the chromosome structural perspective. Converting adult somatic cells to neuron cells, through either reprogramming or transdifferentiation, has been deemed a promising therapeutic strategy for neurodegenerative diseases [84]. Our work presented a computational approach that can be used to dissect pathways and identify intermediate states during neural developmental processes from the chromosome structural perspective. The results serve as a theoretical exploration of the neural cell-fate determination, aiming for the potential applications in neuroregeneration and disease modeling [85].

ACKNOWLEDGMENTS

X.C. acknowledges support from the National Natural Science Foundation of China (Grant No. 32201020), the general program of Guangdong Basic and Applied Basic Research Foundation (Grant No. 2024A1515010862), the general program (Grants No. 2023A04J0083) and the Guangzhou-HKUST(GZ) joint funding program (Grant No. 2023A03J0060) of the Guangzhou Municipal Science and Technology Project. X.C. was also partly supported by the Municipal Key Laboratory Construction program of the Guangzhou Municipal Science and Technology Project (No. 2023A03J0003).

[1] R. Bocchi, G. Masserdotti, and M. Götz, Direct neuronal reprogramming: Fast forward from new concepts toward therapeutic approaches, Neuron **110**, 366 (2022).

[2] C. Jopling, S. Boue, and J. C. I. Belmonte, Dedifferentiation, transdifferentiation and reprogramming: Three routes to regeneration, Nat. Rev. Mol. Cell Biol. **12**, 79 (2011).

[3] T. Vierbuchen, A. Ostermeier, Z. P. Pang, Y. Kokubu, T. C. Südhof, and M. Wernig, Direct conversion of fibroblasts to functional neurons by defined factors, Nature (London) **463**, 1035 (2010).

[4] W. Hu, B. Qiu, W. Guan, Q. Wang, M. Wang, W. Li, L. Gao, L. Shen, Y. Huang, G. Xie *et al.*, Direct conversion of normal and Alzheimers disease human fibroblasts into neuronal cells by small molecules, Cell Stem Cell **17**, 204 (2015).

[5] Y. Yang, R. Chen, X. Wu, Y. Zhao, Y. Fan, Z. Xiao, J. Han, L. Sun, X. Wang, and J. Dai, Rapid and efficient conversion of human fibroblasts into functional neurons by small molecules, Stem Cell Reports **13**, 862 (2019).

[6] Z. Guo, L. Zhang, Z. Wu, Y. Chen, F. Wang, and G. Chen, In vivo direct reprogramming of reactive glial cells into functional neurons after brain injury and in an Alzheimer's disease model, Cell Stem Cell **14**, 188 (2014).

[7] H. Qian, X. Kang, J. Hu, D. Zhang, Z. Liang, F. Meng, X. Zhang, Y. Xue, R. Maimon, S. F. Dowdy *et al.*, Reversing

a model of parkinsons disease with in situ converted nigral neurons, Nature (London) **582**, 550 (2020).

[8] H. Zhou, J. Su, X. Hu, C. Zhou, H. Li, Z. Chen, Q. Xiao, B. Wang, W. Wu, Y. Sun *et al.*, Glia-to-neuron conversion by CRISPR-CasRx alleviates symptoms of neurological disease in mice, Cell **181**, 590 (2020).

[9] L.-L. Wang and C.-L. Zhang, In vivo glia-to-neuron conversion: Pitfalls and solutions, Dev. Neurobiol. **82**, 367 (2022).

[10] S. Gascón, G. Masserdotti, G. L. Russo, and M. Götz, Direct neuronal reprogramming: Achievements, hurdles, and new roads to success, Cell Stem Cell **21**, 18 (2017).

[11] A. M. Oudelaar and D. R. Higgs, The relationship between genome structure and function, Nat. Rev. Genet. **22**, 154 (2021).

[12] J. Dekker, K. Rippe, M. Dekker, and N. Kleckner, Capturing chromosome conformation, Science **295**, 1306 (2002).

[13] E. Lieberman-Aiden, N. L. Van Berkum, L. Williams, M. Imakaev, T. Ragoczy, A. Telling, I. Amit, B. R. Lajoie, P. J. Sabo, M. O. Dorschner *et al.*, Comprehensive mapping of long-range interactions reveals folding principles of the human genome, Science **326**, 289 (2009).

[14] J. R. Dixon, S. Selvaraj, F. Yue, A. Kim, Y. Li, Y. Shen, M. Hu, J. S. Liu, and B. Ren, Topological domains in mammalian genomes identified by analysis of chromatin interactions, Nature (London) **485**, 376 (2012).

[15] E. P. Nora, B. R. Lajoie, E. G. Schulz, L. Giorgetti, I. Okamoto, N. Servant, T. Piolot, N. L. van Berkum, J. Meisig, J. Sedat *et al.*, Spatial partitioning of the regulatory landscape of the X-inactivation centre, Nature (London) **485**, 381 (2012).

[16] T. Sexton, E. Yaffe, E. Kenigsberg, F. Bantignies, B. Leblanc, M. Hoichman, H. Parrinello, A. Tanay, and G. Cavalli, Three-dimensional folding and functional organization principles of the drosophila genome, Cell **148**, 458 (2012).

[17] S. S. Rao, M. H. Huntley, N. C. Durand, E. K. Stamenova, I. D. Bochkov, J. T. Robinson, A. L. Sanborn, I. Machol, A. D. Omer, E. S. Lander *et al.*, A 3D map of the human genome at kilobase resolution reveals principles of chromatin looping, Cell **159**, 1665 (2014).

[18] H. Zheng and W. Xie, The role of 3D genome organization in development and cell differentiation, Nat. Rev. Mol. Cell Biol. **20**, 535 (2019).

[19] R. Stadhouders, G. J. Filion, and T. Graf, Transcription factors and 3D genome conformation in cell-fate decisions, Nature (London) **569**, 345 (2019).

[20] J. R. Dixon, I. Jung, S. Selvaraj, Y. Shen, J. E. Antosiewicz-Bourget, A. Y. Lee, Z. Ye, A. Kim, N. Rajagopal, W. Xie *et al.*, Chromatin architecture reorganization during stem cell differentiation, Nature (London) **518**, 331 (2015).

[21] W. Xie, M. D. Schultz, R. Lister, Z. Hou, N. Rajagopal, P. Ray, J. W. Whitaker, S. Tian, R. D. Hawkins, D. Leung *et al.*, Epigenomic analysis of multilineage differentiation of human embryonic stem cells, Cell **153**, 1134 (2013).

[22] B. Bonev, N. M. Cohen, Q. Szabo, L. Fritsch, G. L. Papadopoulos, Y. Lubling, X. Xu, X. Lv, J.-P. Hugnot, A. Tanay *et al.*, Multiscale 3D genome rewiring during mouse neural development, Cell **171**, 557 (2017).

[23] P. Rajarajan, T. Borrman, W. Liao, N. Schrode, E. Flaherty, C. Casiño, S. Powell, C. Yashaswini, E. A. LaMarca, B. Kassim, B. Javidfar, S. Espeso-Gil, A. Li, H. Won, D. H. Geschwind, S.-M. Ho, M. MacDonald, G. E. Hoffman, P. Roussos, B. Zhang, C.-G. Hahn, Z. Weng, K. J. Brennand, and S. Akbarian, Neuron-specific signatures in the chromosomal connectome associated with schizophrenia risk, Science **362**, eaat4311 (2018).

[24] V. Dileep and L.-H. Tsai, Three-dimensional chromatin organization in brain function and dysfunction, Curr. Opin. Neurobiol. **69**, 214 (2021).

[25] H. Won, L. de La Torre-Ubieta, J. L. Stein, N. N. Parikshak, J. Huang, C. K. Opland, M. J. Gandal, G. J. Sutton, F. Hormozdiari, D. Lu *et al.*, Chromosome conformation elucidates regulatory relationships in developing human brain, Nature (London) **538**, 523 (2016).

[26] A. D. Schmitt, M. Hu, I. Jung, Z. Xu, Y. Qiu, C. L. Tan, Y. Li, S. Lin, Y. Lin, C. L. Barr *et al.*, A compendium of chromatin contact maps reveals spatially active regions in the human genome, Cell Reports **17**, 2042 (2016).

[27] D. Racko, F. Benedetti, D. Goundaroulis, and A. Stasiak, Chromatin loop extrusion and chromatin unknotting, Polymers **10**, 1126 (2018).

[28] X. Chu and J. Wang, Conformational state switching and pathways of chromosome dynamics in cell cycle, Appl. Phys. Rev. **7**, 031403 (2020).

[29] X. Chu and J. Wang, Microscopic chromosomal structural and dynamical origin of cell differentiation and reprogramming, Adv. Sci. **7**, 2001572 (2020).

[30] X. Chu and J. Wang, Deciphering the molecular mechanism of the cancer formation by chromosome structural dynamics, PLoS Comput. Biol. **17**, 1 (2021).

[31] X. Chu and J. Wang, Quantifying chromosome structural reorganization during differentiation, reprogramming, and transdifferentiation, Phys. Rev. Lett. **129**, 068102 (2022).

[32] X. Chu and J. Wang, Dynamics and pathways of chromosome structural organizations during cell transdifferentiation, JACS Au **2**, 116 (2022).

[33] X. Chu and J. Wang, Insights into the cell fate decision-making processes from chromosome structural reorganizations, Biophys. Rev. **3**, 041402 (2022).

[34] X. Chu and J. Wang, Quantifying the large-scale chromosome structural dynamics during the mitosis-to-G1 phase transition of cell cycle, Open Biol. **13**, 230175 (2023).

[35] N. Servant, N. Varoquaux, B. R. Lajoie, E. Viara, C.-J. Chen, J.-P. Vert, E. Heard, J. Dekker, and E. Barillot, HiC-Pro: An optimized and flexible pipeline for Hi-C data processing, Genome Biol. **16**, 259 (2015).

[36] M. Imakaev, G. Fudenberg, R. P. McCord, N. Naumova, A. Goloborodko, B. R. Lajoie, J. Dekker, and L. A. Mirny, Iterative correction of Hi-C data reveals hallmarks of chromosome organization, Nat. Methods **9**, 999 (2012).

[37] F. Benedetti, J. Dorier, Y. Burnier, and A. Stasiak, Models that include supercoiling of topological domains reproduce several known features of interphase chromosomes, Nucl. Acids Res. **42**, 2848 (2014).

[38] B. Zhang and P. G. Wolynes, Shape transitions and chiral symmetry breaking in the energy landscape of the mitotic chromosome, Phys. Rev. Lett. **116**, 248101 (2016).

[39] A. Rosa and R. Everaers, Structure and dynamics of interphase chromosomes, PLoS Comput. Biol. **4**, e1000153 (2008).

[40] H. R. Warner Jr, Kinetic theory and rheology of dilute suspensions of finitely extensible dumbbells, Ind. Eng. Chem. Fund. **11**, 379 (1972).

[41] N. Naumova, M. Imakaev, G. Fudenberg, Y. Zhan, B. R. Lajoie, L. A. Mirny, and J. Dekker, Organization of the mitotic chromosome, Science **342**, 948 (2013).

[42] B. Zhang and P. G. Wolynes, Topology, structures, and energy landscapes of human chromosomes, Proc. Natl. Acad. Sci. USA **112**, 6062 (2015).

[43] A. Cesari, S. Reißer, and G. Bussi, Using the maximum entropy principle to combine simulations and solution experiments, Computation **6**, 15 (2018).

[44] Y. Qi, A. Reyes, S. E. Johnstone, M. J. Aryee, B. E. Bernstein, and B. Zhang, Data-driven polymer model for mechanistic exploration of diploid genome organization, Biophys. J. **119**, 1905 (2020).

[45] F. Uhlmann, SMC complexes: From DNA to chromosomes, Nat. Rev. Mol. Cell Biol. **17**, 399 (2016).

[46] B. Hess, C. Kutzner, D. Van Der Spoel, and E. Lindahl, Gromacs 4: Algorithms for highly efficient, load-balancing, and scalable molecular simulation, J. Chem. Theory Comput. **4**, 435 (2008).

[47] G. A. Tribello, M. Bonomi, D. Branduardi, C. Camilloni, and G. Bussi, PLUMED 2: New feathers for an old bird, Comput. Phys. Commun. **185**, 604 (2014).

[48] T. Nagano, Y. Lubling, T. J. Stevens, S. Schoenfelder, E. Yaffe, W. Dean, E. D. Laue, A. Tanay, and P. Fraser, Single-cell Hi-C reveals cell-to-cell variability in chromosome structure, Nature (London) **502**, 59 (2013).

[49] S. Bianco, D. G. Lupiáñez, A. M. Chiariello, C. Annunziatella, K. Kraft, R. Schöpflin, L. Wittler, G. Andrey, M. Vingron, A. Pombo *et al.*, Polymer physics predicts the effects of structural variants on chromatin architecture, Nat. Genet. **50**, 662 (2018).

[50] E. Crane, Q. Bian, R. P. McCord, B. R. Lajoie, B. S. Wheeler, E. J. Ralston, S. Uzawa, J. Dekker, and B. J. Meyer, Condensin-driven remodelling of X chromosome topology during dosage compensation, Nature (London) **523**, 240 (2015).

[51] B. Zhang and P. G. Wolynes, Genomic energy landscapes, Biophys. J. **112**, 427 (2017).

[52] See Supplemental Material at http://link.aps.org/supplemental/10.1103/PhysRevResearch.6.023309 for additional figures.

[53] D. L. Spector, The dynamics of chromosome organization and gene regulation, Annu. Rev. Biochem. **72**, 573 (2003).

[54] R. Schneider and R. Grosschedl, Dynamics and interplay of nuclear architecture, genome organization, and gene expression, Genes Dev. **21**, 3027 (2007).

[55] A. Smallwood and B. Ren, Genome organization and long-range regulation of gene expression by enhancers, Curr. Opin. Cell Biol. **25**, 387 (2013).

[56] D. U. Gorkin, D. Leung, and B. Ren, The 3D genome in transcriptional regulation and pluripotency, Cell Stem Cell **14**, 762 (2014).

[57] V. Martínez-Cerdeño and S. C. Noctor, Neural progenitor cell terminology, Front. Neuroanat. **12**, 104 (2018).

[58] P. H. L. Krijger, B. Di Stefano, E. de Wit, F. Limone, C. Van Oevelen, W. De Laat, and T. Graf, Cell-of-origin-specific 3D genome structure acquired during somatic cell reprogramming, Cell Stem Cell **18**, 597 (2016).

[59] B. Treutlein, Q. Y. Lee, J. G. Camp, M. Mall, W. Koh, S. A. M. Shariati, S. Sim, N. F. Neff, J. M. Skotheim, M. Wernig *et al.*, Dissecting direct reprogramming of fibroblast to neuron using single-cell RNA-seq, Nature (London) **534**, 391 (2016).

[60] J. Wang, K. Zhang, L. Xu, and E. Wang, Quantifying the waddington landscape and biological paths for development and differentiation, Proc. Natl. Acad. Sci. USA **108**, 8257 (2011).

[61] A. L. Sanborn, S. S. Rao, S.-C. Huang, N. C. Durand, M. H. Huntley, A. I. Jewett, I. D. Bochkov, D. Chinnappan, A. Cutkosky, J. Li *et al.*, Chromatin extrusion explains key features of loop and domain formation in wild-type and engineered genomes, Proc. Natl. Acad. Sci. USA **112**, E6456 (2015).

[62] G. Fudenberg, M. Imakaev, C. Lu, A. Goloborodko, N. Abdennur, and L. A. Mirny, Formation of chromosomal domains by loop extrusion, Cell Rep. **15**, 2038 (2016).

[63] A. Boija, I. A. Klein, B. R. Sabari, A. Dall'Agnese, E. L. Coffey, A. V. Zamudio, C. H. Li, K. Shrinivas, J. C. Manteiga, N. M. Hannett *et al.*, Transcription factors activate genes through the phase-separation capacity of their activation domains, Cell **175**, 1842 (2018).

[64] A. G. Larson, D. Elnatan, M. M. Keenen, M. J. Trnka, J. B. Johnston, A. L. Burlingame, D. A. Agard, S. Redding, and G. J. Narlikar, Liquid droplet formation by HP1α suggests a role for phase separation in heterochromatin, Nature (London) **547**, 236 (2017).

[65] A. R. Strom, A. V. Emelyanov, M. Mir, D. V. Fyodorov, X. Darzacq, and G. H. Karpen, Phase separation drives heterochromatin domain formation, Nature (London) **547**, 241 (2017).

[66] C. H. Waddington, *The Strategy of the Genes* (Routledge, London, 1957).

[67] K. Takahashi and S. Yamanaka, Induction of pluripotent stem cells from mouse embryonic and adult fibroblast cultures by defined factors, Cell **126**, 663 (2006).

[68] K. Takahashi, K. Tanabe, M. Ohnuki, M. Narita, T. Ichisaka, K. Tomoda, and S. Yamanaka, Induction of pluripotent stem cells from adult human fibroblasts by defined factors, Cell **131**, 861 (2007).

[69] P. Hou, Y. Li, X. Zhang, C. Liu, J. Guan, H. Li, T. Zhao, J. Ye, W. Yang, K. Liu *et al.*, Pluripotent stem cells induced from mouse somatic cells by small-molecule compounds, Science **341**, 651 (2013).

[70] Y. Zhao, T. Zhao, J. Guan, X. Zhang, Y. Fu, J. Ye, J. Zhu, G. Meng, J. Ge, S. Yang *et al.*, A XEN-like state bridges somatic cells to pluripotency during chemical reprogramming, Cell **163**, 1678 (2015).

[71] J. Guan, G. Wang, J. Wang, Z. Zhang, Y. Fu, L. Cheng, G. Meng, Y. Lyu, J. Zhu, Y. Li *et al.*, Chemical reprogramming of human somatic cells to pluripotent stem cells, Nature (London) **605**, 325 (2022).

[72] K. Hochedlinger and K. Plath, Epigenetic reprogramming and induced pluripotency, Development **136**, 509 (2009).

[73] X. Fang, K. Kruse, T. Lu, and J. Wang, Nonequilibrium physics in biology, Rev. Mod. Phys. **91**, 045004 (2019).

[74] C. R. Clapier and B. R. Cairns, The biology of chromatin remodeling complexes, Annu. Rev. Biochem. **78**, 273 (2009).

[75] G. J. Narlikar, R. Sundaramoorthy, and T. Owen-Hughes, Mechanisms and functions of ATP-dependent chromatin-remodeling enzymes, Cell **154**, 490 (2013).

[76] K. Kremer, G. S. Grest, and I. Carmesin, Crossover from rouse to reptation dynamics: A molecular-dynamics simulation, Phys. Rev. Lett. **61**, 566 (1988).

[77] J. T. Kalathi, S. K. Kumar, M. Rubinstein, and G. S. Grest, Rouse mode analysis of chain relaxation in homopolymer melts, Macromolecules **47**, 6925 (2014).

[78] K. Abramo, A.-L. Valton, S. V. Venev, H. Ozadam, A. N. Fox, and J. Dekker, A chromosome folding intermediate at the condensin-to-cohesin transition during telophase, Nat. Cell Biol. **21**, 1393 (2019).

[79] H. Zhang, D. J. Emerson, T. G. Gilgenast, K. R. Titus, Y. Lan, P. Huang, D. Zhang, H. Wang, C. A. Keller, B. Giardine *et al.*, Chromatin structure dynamics during the mitosis-to-G1 phase transition, Nature (London) **576**, 158 (2019).

[80] T. Graf, Historical origins of transdifferentiation and reprogramming, Cell Stem Cell **9**, 504 (2011).

[81] J. Xu, Y. Du, and H. Deng, Direct lineage reprogramming: Strategies, mechanisms, and applications, Cell Stem Cell **16**, 119 (2015).

[82] A. Cieślar-Pobuda, V. Knoflach, M. V. Ringh, J. Stark, W. Likus, K. Siemianowicz, S. Ghavami, A. Hudecki, J. L. Green, and M. J. Łos, Transdifferentiation and reprogramming: Overview of the processes, their similarities and differences, Biochim. Biophys. Acta **1864**, 1359 (2017).

[83] A. Reid and B. Tursun, Transdifferentiation: Do transition states lie on the path of development? Curr. Opin. Syst. Biol. **11**, 18 (2018).

[84] C. Mollinari, J. Zhao, L. Lupacchini, E. Garaci, D. Merlo, and G. Pei, Transdifferentiation: A new promise for neurodegenerative diseases, Cell Death Dis. **9**, 830 (2018).

[85] C. Feng, J. Wang, and X. Chu, Large-scale data-driven and physics-based models offer insights into the relationships among the structures, dynamics, and functions of the chromosomes, J. Mol. Cell Biol. **15**, mjad042 (2023).